Reaction pathways towards the formation of dolomite-analogues at ambient conditions Carlos Pimentel, Carlos M. Pina *

Departamento de Cristalografía y Mineralogía, Facultad de Ciencias Geológicas, Universidad Complutense de Madrid, c/ José Antonio Novais, 2, E-28040 Madrid, Spain
Instituto de Geociencias IGEO (UCM – CSIC), E-28040 Madrid, Spain

Abstract

In this paper we present results of a study of the crystallisation behaviour of the dolomite-analogues norsethite and PbMg $(CO_3)_2$ at room temperature and atmospheric pressure. Whereas precipitation of norsethite was previously obtained by mix-ing solutions (Hood et al., 1974; Pimentel and Pina, 2014a,b), we report, for the first time, the synthesis of $PbMg(CO_3)_2$ by using the same method. The formation of both phases was promoted by ageing slurries for periods of time ranging from a few days (norsethite) up to 6 months ($PbMg(CO_3)_2$). The crystallisation of both norsethite and $PbMg(CO_3)_2$ occurs by sequences of dissolution–precipitation reactions involving several amorphous and crystalline precursor phases, which were identified and characterised by X-ray diffraction and scanning electron microscopy. Depending on the initial composition and Ba:Mg and Pb:Mg ratios in the slurries, different precursors and reaction kinetics were observed. This demonstrates the existence of different reaction pathways towards the formation of the investigated dolomite-analogues. Our experimental results provide new insights into the possible mechanisms of formation of dolomite and other double carbonates in nature.

1. INTRODUCTION

Unlike dolomite $(CaMg(CO_3)_2)$ the analogous com-pounds norsethite $(BaMg(CO_3)_2)$ and $PbMg(CO_3)_2$ can be easily obtained in the laboratory under ambient conditions (Lippmann, 1973; Hood et al., 1974; Morrow and Ricketts, 1986; Bo¨ttcher et al., 1997; Bo¨ttcher, 2000; Deelman, 2011; Pimentel and Pina, 2014a,b). Nevertheless, previous investi-gations have revealed that norsethite and $PbMg(CO_3)_2$ can-not be formed directly from aqueous solutions and their crystallisation requires the transformation of amorphous/crystalline precursors (Lippmann, 1973; Hood et al., 1974; Morrow and Ricketts, 1986; Pimentel and Pina, 2014a,b). The presence of precursors has also been identified in exper-iments designed to synthesise dolomite from hydrothermal solutions (Kelleher and Redfern, 2002; Rodriguez-Blanco et al., 2015). This suggests the existence of a common mech-anism for the formation of dolomite and its analogues, which essentially differ in their kinetics. Assuming the valid-ity of this scenario, we argue that an investigation of the reaction paths to the formation of norsethite and PbMg $(CO_3)_2$ is relevant for solving the long-standing ‘‘dolomite problem”, i.e. the determination of the reaction (or reac-tions) for the formation of dolomite in nature under ambi-ent conditions.

Norsethite and $PbMg(CO_3)_2$ crystallise in the space group R32 with the following hexagonal unit cell parame-ters: a = 0.5017 nm and c = 1.677 nm for norsethite; and a = 0.4924 nm and c = 1.656 nm for $PbMg(CO_3)_2$ (Lippmann, 1973). Given that the radii of Ba^{2+} (1.38 Å)

* Corresponding author at: Departamento de Cristalografı´a y Mineralogı´a, Facultad de Ciencias Geolo´gicas, Universidad Complutense de Madrid, c/ Jose´ Antonio Novais, 2, E-28040 Madrid, Spain.
E-mail address: cmpina@geo.ucm.es (C.M. Pina).

and Pb^{2+} (1.26 ˚A) are significantly larger than the radius of Ca^{2+} (1.04 A˚), the orientation of the carbonate groups in the structures of norsethite and $PbMg(CO_3)_2$ is slightly different than in dolomite, which crystallises in the less sym-metric space group R□3. In view of these minor structural differences, Lippmann (1966) defined norsethite and $PbMg(CO_3)_2$ as dolomite-homotypes. In the dolomite, nor-sethite and $PbMg(CO_3)_2$ structures, layers of Mg^{2+} alter-nate along the c axis with layers of Ca^{2+}, B a $^{2+}$ and Pb^{2+}, respectively. This cationic ordering results in characteristic superstructure diffraction peaks with indexes h0.l and 0k.l (l = odd-number). Previous studies have shown that the cationic ordering in this family of structures can be quanti-fied by calculating relative intensities of superstructure peaks (McKenzie, 1981; Schultz-Gu¨ttler, 1986; Pimentel and Pina, 2014a). Interestingly, variations in the relative intensity of these superstructure peaks can be used to mon-itor changes in cationic order during the formation of dolo-mite and dolomite-analogues (e.g. Pimentel and Pina, 2014a; Rodriguez-Blanco et al., 2015), as well as to detect ordering–disordering phenomena when dolomite crystals are subjected to thermal treatments (e.g. Schultz-Gu¨ttler, 1986; Crespo et al., 2015).

The first synthesis of norsethite at room temperature and ambient pressure was reported by Lippmann (1967), who obtained this dolomite-analogue by immersing witherite ($BaCO_3$) powder in aqueous solutions bearing $MgCl_2$ and Na_2CO_3 for a few days. Similarly, Lippmann (1966) precipi-tated $PbMg(CO_3)_2$ by substituting cerussite ($PbCO_3$) powder for witherite in his experiments. Although the synthesis pro-cedure was the same as that for norsethite, $PbMg(CO_3)_2$ was obtained only after 6 months of reaction with the $MgCl_2$–Na_2CO_3 aqueous solutions. The experimental protocol reported by Lippmann (1967) was also used by Morrow and Ricketts (1986) to produce norsethite and $PbMg(CO_3)_2$ at temperatures ranging from 25 to 80 □ C. The results reported by Morrow and Rickets (1986) confirmed that these two dolomite analogues formed with different kinetics.

Alternatively, Hood et al. (1974) proposed an experi-mental protocol to synthesise norsethite by mixing two solutions. In their experiments, solutions of $BaCl_2$–$MgCl_2$ and of Na_2CO_3 were mixed in a vessel to obtain a gel-like phase. After 24 h of ageing, norsethite was the only phase identified by powder X-ray diffraction. This experimental protocol was also successfully used by Bo¨ttcher et al. (1997), Bo¨ttcher (2000), and Pimentel and Pina (2014a,b) to obtain highly crystalline norsethite. However, the synthe-sis of $PbMg(CO_3)_2$ by mixing of solutions at ambient con-ditions has not been reported so far.

Here, we present an investigation of the formation of the dolomite analogues norsethite and $PbMg(CO_3)_2$, based on the experimental protocol proposed by Hood et al.(1974), and recently used by Pimentel and Pina (2014a,b) to identify some precursors of norsethite. Our experiments allowed us to synthesise, for the first time, $PbMg(CO_3)_2$ from mixing solutions at room temperature. Furthermore, our results demonstrate that different reaction pathways to the formation of norsethite and $PbMg(CO_3)_2$ are possi-ble, i.e. these two dolomite-analogues can crystallise from different precursor assemblages. Even though in our experiments both concentrations of ions in the solutions and supersaturation levels with respect to precursors and dolomite-like phases are higher than those of most natural environments, findings reported and discussed in this paper provide new insights into the mechanisms of formation of double carbonates with a dolomite-like structure. We propose that similar formation mechanisms can lead to the crystallisation of dolomite in nature at ambient conditions.

2. EXPERIMENTAL PROCEDURE

Norsethite and $PbMg(CO_3)_2$ were synthesised at room temperature by adding 25 mL of a solution B to 25 mL of a solution A previously placed in plastic beakers. Table 1 shows the composition of the A and B solutions used for these synthesis experiments.

Immediately after mixing, formation of gel-like precipi-tates was observed. The initial pH of the slurries was mea-sured with a pH-metre (USB DrDAQ Data Logger, Pico Technology) equipped with a recording system (PicoLog 5). Electrode calibration was conducted using standard buf-fer solutions of pH 4.01, 7.00 and 9.21. Then, beakers were hermetically closed to prevent subsequent equilibration of the slurries with the atmosphere and stirred for about a minute before they were aged at room temperature. Precip-itates were removed from the beakers at fixed periods of time ranging from one hour to days over the next 6 months. After removal, precipitates were filtered using standard filter paper (Filtros Anoia. S.A.) and dried without previous washing at room temperature. Aliquots of the precipitates were ground and sieved to a particle size <53 lm and subsequently analysed with X-ray powder diffraction (Siemens D-500 diffractometer with a CuKa source). Collected diffractograms were analysed using the XPowder software and the phases were identified using the PDF2 database. Although the evaporation of residual solutions in the pre-cipitates can lead to a subsequent spurious precipitation of small amounts of highly soluble salts (e.g. $NaNO_3$), such salts are easily identified in the diffractograms. The crys-tallinity of norsethite and $PbMg(CO_3)_2$ was quantified through the full width half maximum of the 10.4 diffraction peaks ($FWHM_{10.4}$), and cationic ordering was charac-terised by calculating intensity ratios of selected structure and superstructure reflections: $I_{10.1}/I_{01.2}$ and $I_{01.5}/I_{11.0}$ (McKenzie, 1981; Pimentel and Pina, 2014a).

In order to better visualise the phase evolution in the experiments, the two-dimensional stacking tool of the XPowder software was used (Martin, 2008). Two-dimensional stacking of diffractograms for the whole reac-tion time for each experiment allowed us to monitor changes in the intensity and width of the diffraction peaks of both precursor and final phases. Relative amounts of the identi-fied phases in the precipitates were calculated using the RIR (reflectivity intensity ratio) tool available in the XPow-der software (Chung, 1974; Hubbard and Snyder, 1988). The RIR method consists in fitting by non-linear least squares a whole diffractogram to a weighted combination of diffraction patterns from the PDF2 database (Martin, 2008). By doing that, weight percentages of the phases pre-sent in a given diffractogram can be estimated.

Table 1
Concentration of the solutions used in the experiments for crystallising norsethite and $PbMg(CO_3)_2$.

	Solution A			Solution B
	$Ba(NO_3)_2$ (mol/L)	$Pb(NO_3)_2$ (mol/L)	$Mg(NO_3)_2$ (mol/L)	Na_2CO_3 (mol/L)
Exp. Ba1	0.06	–	0.1	0.5
Exp. Ba2	0.02	–	0.1	0.5
Exp. Pb1	–	0.06	0.1	0.5
Exp. Pb2	–	0.02	0.1	0.5

A selected number of precipitates were also imaged and chemically analysed with a scanning electron microscope (SEM, JEOL JSM 6400-40kV) equipped with a Link-analytical Energy Dispersive X-ray Analysis (EDX) system.

3. RESULTS

3.1. Formation of norsethite

In all experiments, norsethite did not directly precipitate upon mixing of the $Ba(NO_3)_2$–$Mg(NO_3)_2$ and Na_2CO_3 solutions. In turn, the instantaneous formation of gel-like slurries after solution mixing was observed. The pH values measured just after mixing the solutions were: 11.0 for Exp. Ba1 and 10.8 for Exp. Ba2. Table 2 shows the initial satu-ration states of the solutions with respect to the phases subsequently identified by X-ray diffraction.

As can be seen in Table 2, the resulting solutions imme-diately after mixing are highly supersaturated with respect to hydromagnesite, norsethite and witherite, moderately supersaturated with respect to nesquehonite and undersatu-rated for eitelite. However, gel-like slurries are not formed by assemblages of the phases for which supersaturation val-ues are the highest but by complex mixtures of amorphous and crystalline phases. The formation of these gel-like slur-ries is the starting point for dissolution–crystallisation reac-tions involving a number of precursors which eventually lead to the formation of highly crystalline norsethite with a high degree of Ba–Mg ordering (see Table 3, Fig. 1 and Fig. EA-1 in the Electronic Annex).

Depending on the concentration and Ba:Mg ratio of the solutions, both the precursor phases and the reaction kinet-ics towards the formation of norsethite vary. In Table 3, the possible precursor phases and the times for detection of first and highly crystalline norsethite are listed. Fig. 2 shows the time evolution of the main diffraction peaks of norsethite. For an initial Ba:Mg ratio of 0.6 (Exp. Ba1), norsethite is formed in the first 2 h of slurry ageing and in about 24 h its crystallinity rapidly increases from $FWHM_{10.4}$ = 1.98 to $FWHM_{10.4}$ = 0.38. When the initial Ba:Mg is reduced to 0.2 (Exp. Ba2), the formation of norsethite also occurs within the first 2 h of slurry ageing, but in contrast with Exp. Ba1, the crystallinity of this mineral phase remains relatively low for a longer period of time. Only after ageing for more than 72 h does the norsethite become highly crys-talline with an average value of 0.34 for $FWHM_{10.4}$. The degree of cationic ordering of norsethite does not signifi-cantly change with the ageing process, regardless of the initial concentration of the solutions. Ordering indexes were almost constant values from the first detection of norsethite in the precipitates: $I_{10.1}/I_{01.2}$ = 0.93 ± 0.10 and $I_{01.5}/I_{11.0}$ = 1.01 ± 0.15. Altogether these results indicate that the Ba–Mg ordering during the crystallisation of norsethite is a relatively fast process compared with the growth of coherent domains.

As can be seen in Fig. 2 and Table 3, differences in Ba: Mg ratios in the initial aqueous solutions do not only affect the kinetics of norsethite formation but also the formation of other phases. Besides an amorphous phase, which is always present as a precursor of norsethite, variable amounts of nitratine ($NaNO_3$) appear as a consequence of the drying process of the samples. The amorphous phase is a precursor whose composition is determined by the com-position of the initial mixing solutions and, subsequently, by the formation and evolution of crystalline phases. Depending on the Ba:Mg ratio, different crystalline phases have been detected (see Electronic Annex, Fig. EA-2). At the high Ba:Mg ratio (Exp. Ba1), peaks of witherite were identified in the diffractograms recorded within the first 24 h of ageing (Fig. 2A). In contrast, at the low Ba:Mg ratio (Exp. Ba2), no witherite was identified in the diffractograms (Fig. 2B), but other phases such as eitelite ($Na_2Mg(CO_3)_2$), hydromagnesite ($Mg_5(CO_3)_4(OH)_2{\cdot}4H_2O$) and nesque-honite ($MgCO_3{\cdot}3H_2O$) were often observed (see Electronic Annex, Fig. EA-2).

Fig. 3 shows the evolution of weight% of the main phases in Exp. Ba1 and Exp. Ba2 during ageing, as calculated from the diffractograms by using the reflectivity

Table 2
Initial saturation states with respect to the crystalline phases in Exp. Ba1 and Exp. Ba2. Supersaturations were calculated using the general expression $b = IAP/K_{sp}$, where IAP is the product of the ionic activities, and K_{sp} the solubility product of each phase. Ionic activities were calculated using the ''WATEQ" Debye–Hu¨ckel formalism available in the PHREEQC computer code for chemical speciation of aqueous solutions (Parkhurst and Appelo, 2013), and the solubility products were taken from the literature or calculated from reported free energies of formation (see Electronic Annex for further details on the K_{sp} calculations).

Experiment/supersaturation	[b]Hydromagnesite	[b]Norsethite	[b]Witherite	[b]Nesquehonite	[b]Eitelite
Exp. Ba1	$2.3{\cdot}10^{12}$	$3.7{\cdot}10^{7}$	$1.6{\cdot}10^{4}$	2.3	$2.0{\cdot}10^{-4}$
Exp. Ba2	$3.6{\cdot}10^{12}$	$1.6{\cdot}10^{7}$	$5.3{\cdot}10^{3}$	3.0	$3.0{\cdot}10^{-4}$

Table 3

Experiments for crystallising norsethite: Ba:Mg ratio in the solutions, possible precursor phases identified by X-ray diffraction, time for first observation of norsethite and time for highly crystalline norsethite. Concentrations of the solutions for Exp. Ba1 and Exp. Ba2 are shown in Table 1.

	Ba:Mg	Possible precursors	Time for first norsethite (hours)	Time for highly crystalline norsethite (hours)
Exp. Ba1	0.6	Amorphous; witherite 0.2	<2	24
Exp. Ba2		Amorphous; eitelite	<2	72

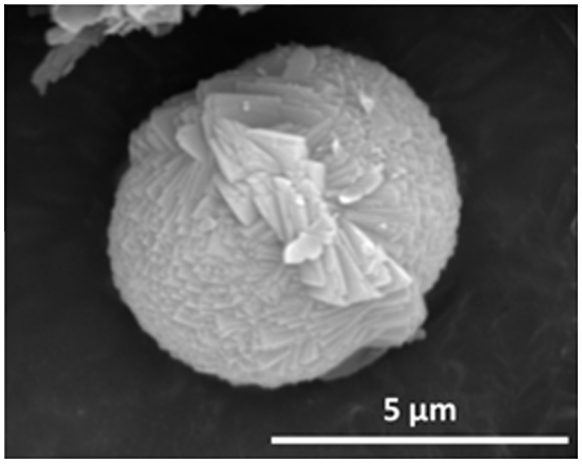

Fig. 1. SEM image of a typical spherulite of norsethite constituted by an aggregate of rhombohedral crystals formed after 14 days of slurry ageing (Exp. Ba2).

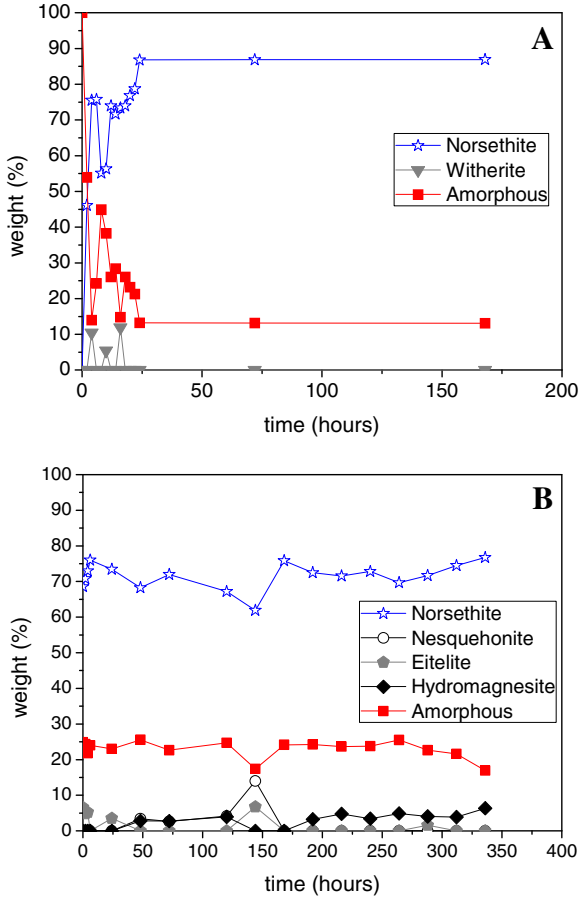

Fig. 3. Time evolution of weight% of the solid phases for (A) Exp. Ba1; and (B) Exp. Ba2. Since nitratine appears as a result of the drying of the precipitates, it has been removed from the plots.

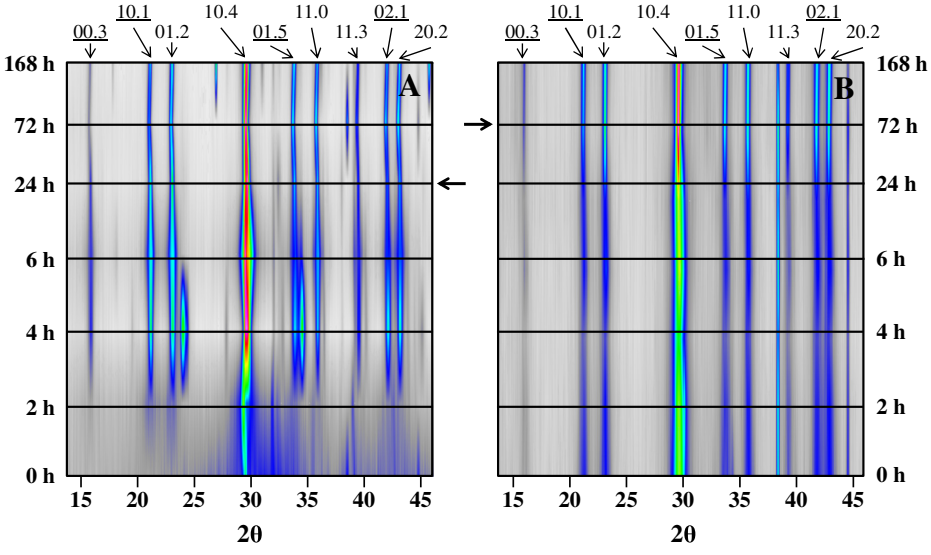

Fig. 2. Two-dimensional stacking of diffractograms taken during the ageing of slurries formed after solution mixing: (A) Exp. Ba1; and (B) Exp. Ba2. Main peaks of norsethite are indicated in both two-dimensional stackings. Underlined peaks indicate norsethite superstructure reflections. Horizontal arrows show times from which highly crystalline norsethite was observed.

intensity ratio (RIR) method (Hubbard and Snyder, 1988). Although the RIR method is semi-quantitative and weight percentages shown in Fig. 3 must be taken with caution, some relevant information can be obtained. In both exper-iments, before reaching a steady state, we observe a period of oscillations in the amounts of the amorphous phase, nor-sethite, and, to a lesser extent, witherite or eitelite. These oscillations can be related to the coupling of dissolution–c rystallisation reactions involving the precursor phases and the final product (norsethite). In addition, the time of oscil-lations is longer in the Exp. Ba2 than in the Exp. Ba1. This indicates that such oscillations are sensitive to the initial conditions (i.e. composition and Ba:Mg ratio in the aque-ous solutions).

3.2. Formation of $PbMg(CO_3)_2$

$PbMg(CO_3)_2$ was formed by ageing of slurries obtained by mixing solutions, as in the case of norsethite. Immedi-ately after mixing the $Pb(NO_3)_2$–$Mg(NO_3)_2$ and Na_2CO_3 solutions, the formation of a gel-like phase was again observed. The pH values measured after mixing the solu-tions were: 10.8 for Exp. Pb1 and 10.7 for Exp. Pb2. Table 4 shows supersaturation values at the moment of the forma-tion of the gel-like slurries. As can be seen in this table, whereas the highest supersaturation values correspond to $NaPb_2(CO_3)_2OH$, hydromagnesite, hydrocerussite and $PbMg(CO_3)_2$, supersaturations with respect to the rest of the identified crystalline phases are much lower (i.e. nesque-honite in Exp. Pb1 and Exp. Pb2, and cerussite in Exp. Pb1) or the solutions are even undersaturated for some of them (hydrocerussite and cerussite in Exp. Pb2). However, initial precipitates do not contain either hydromagnesite or $PbMg(CO_3)_2$ and the initial composition of the slurries cannot be explained in terms of the supersaturations listed in Table 4. Unlike the experiments described in the previous sec-tion, the formation of $PbMg(CO_3)_2$ involved a higher num-ber of precursor crystalline phases (see column 3 in Table 5 and Fig. EA-4 in the Electronic Annex). In addition, we observed that the time required for the formation of $PbMg(CO_3)_2$ strongly depends on the Pb:Mg ratio of the initial solutions. Whereas at Pb:Mg ratio of 0.6, $PbMg(CO_3)_2$ appeared after 2–3 months of slurry ageing (Exp. Pb1), an initial Pb:Mg ratio of 0.2 resulted in the formation of $PbMg(CO_3)_2$ about 7 days after mixing the solutions (Exp. Pb2). Remarkably, once $PbMg(CO_3)_2$ appears, its degree of crystallinity and cationic ordering do not signifi-cantly change with the ageing process. For the $PbMg(CO_3)_2$ crystals obtained from Exp. Pb1 and Exp. Pb2 (Fig. 4), the average $FWHM_{10.4}$ is 0.23 ± 0.02 and the aver-age of the cationic ordering indexes are $I_{10.1}/I_{01.2}$ = 0.96± 0.06 and $I_{01.5}/I_{11.0}$ = 1.16 ± 0.19. This indicates that Pb–Mg ordering during the formation of $PbMg(CO_3)_2$ occurs simultaneously to the development of large coherent domains within the crystals.

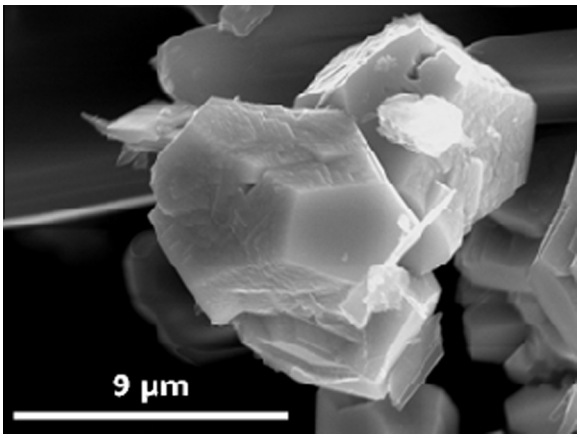

Fig. 4. SEM image of $PbMg(CO_3)_2$ crystals with pseudo-dodecahedral morphologies defined by a combination of {10.4} and {01.1} forms. These singular morphologies have also been observed in calcite crystals and they have been interpreted as the result of the stabilisation of {01.1} forms by a variety of additives, including Mg^{2+} (Song et al., 2009).

In the two experiments conducted to synthesise $PbMg(CO_3)_2$, an almost identical assemblage of precursor phases was identified: $NaPb_2(CO_3)_2OH$ as a major phase, and nesquehonite and lead carbonates (hydrocerussite in Exp.

Table 4
Initial saturation states with respect to the crystalline phases in Exp. Pb1 and Exp. Pb2. Supersaturations were calculated using the general expression b = IAP/K_{sp}, where IAP is the product of the ionic activities, and K_{sp} the solubility product of each phase. Ionic activities were calculated using the ''WATEQ" Debye–Hu¨ckel formalism available in the PHREEQC computer code for chemical speciation of aqueous solutions (Parkhurst and Appelo, 2013), and solubility products were taken from the literature or calculated from reported free energies of formation (see Electronic Annex for further details on the K_{sp} calculations).

Experiment/supersaturation	$b_{NaPb_2(CO_3)_2OH}$	$b_{Hydromagnesite}$	$b_{PbMg(CO_3)_2}$	$b_{Nesquehonite}$	$b_{Hydrocerussite}$	$b_{Cerussite}$
Exp. Pb1	$7.6\cdot10^{21}$	$4.6\cdot10^{12}$	$3.4\cdot10^{3}$	4.9	$2.1\cdot10^{4}$	1.1
Exp. Pb2	$7.6\cdot10^{18}$	$4.8\cdot10^{12}$	58.9	3.8	0.9	0.02

Table 5
Experiments for crystallising $PbMg(CO_3)_2$: Pb:Mg ratio in the solutions, possible precursor phases identified by X-ray diffraction and time for first clear observation of $PbMg(CO_3)_2$. Concentrations of the solutions for Exp. Pb1 and Exp. Pb2 are shown in Table 1.

	Pb:Mg	Possible Precursors	Time for first $PbMg(CO_3)_2$ (days)
Exp. Pb1	0.6	Amorphous; nesquehonite; hydrocerussite; $NaPb_2(CO_3)_2OH$	60–90
Exp. Pb2	0.2	Amorphous; nesquehonite; cerussite; $NaPb_2(CO_3)_2OH$	~7

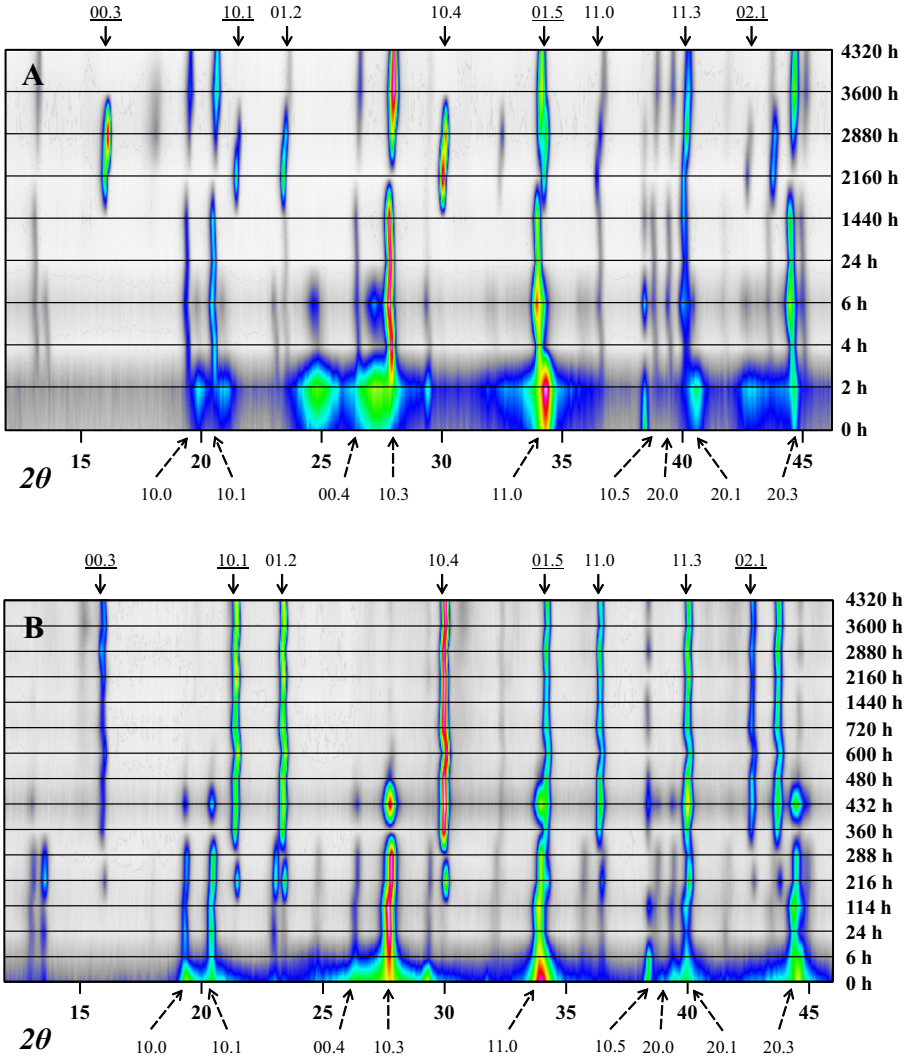

Fig. 5. Two-dimensional stacking of diffractograms taken during the ageing of slurries formed after solution mixing: (A) Exp. Pb1; and (B) Exp. Pb2. Main peaks of $PbMg(CO_3)_2$ are indicated by solid arrows. Underlined peaks indicate superstructure reflections. Peaks of $NaPb_2(CO_3)_2OH$ are indicate by dashed arrows.

Pb1 and cerussite in Exp. Pb2) as minor phases. Fig. 5 shows the evolution of the diffraction peaks of $PbMg(CO_3)_2$ in both experiments. In Exp. Pb1, $PbMg(CO_3)_2$ starts to dissolve after 1 month of its first detection in favour of the precursor phase $NaPb_2(CO_3)_2OH$. $PbMg(CO_3)_2$ completely disappears after 2 months of its first identification in the diffractograms (Fig. 5A). In contrast, $PbMg(CO_3)_2$ is predominant in Exp. Pb2 after about one month of chemical evolution, in which $NaPb_2(CO_3)_2OH$ or $PbMg(CO_3)_2$ are identified as major phases (Fig. 5B).

The evolution of the solid phases in Exp. Pb1 and Exp. Pb2 is better visualised in the RIR plots (Fig. 6). As can be seen in Fig. 6A (Exp. Pb1), in the first hours of ageing, hydrocerussite and an amorphous phase are precursors of $NaPb_2(CO_3)_2OH$, and nesquehonite appears as a minor phase. As in the case of the experiments for crystallising norsethite, the amorphous phase has a variable composition, which depends on both the initial composition of the mixing solutions and the subsequent phase evolution in the system. After 24 h, hydrocerussite and nesquehonite disappear. This leads to an increase of dissolved Mg^{2+} and Pb^{2+}, which is followed by the precipitation of a large amount of $NaPb_2(CO_3)_2OH$. In contrast, in Exp. Pb2, where the Pb:Mg ratio is 0.2, $NaPb_2(CO_3)_2OH$, nesque-honite, cerussite and an amorphous phase are present in the first days of ageing (Fig. 6B). Due to low Pb:Mg ratio, during the early stages of the $PbMg(CO_3)_2$ formation, nesquehonite remains as a minor phase. Furthermore, large oscillations in the relative amounts of these precursor phases occur during the first month of ageing, i.e. for a longer period of time than those observed during the formation of norsethite (Exp. Ba1 and Exp. Ba2). After one month of ageing, hydromagnesite but no nesquehonite was detected in the diffractograms.

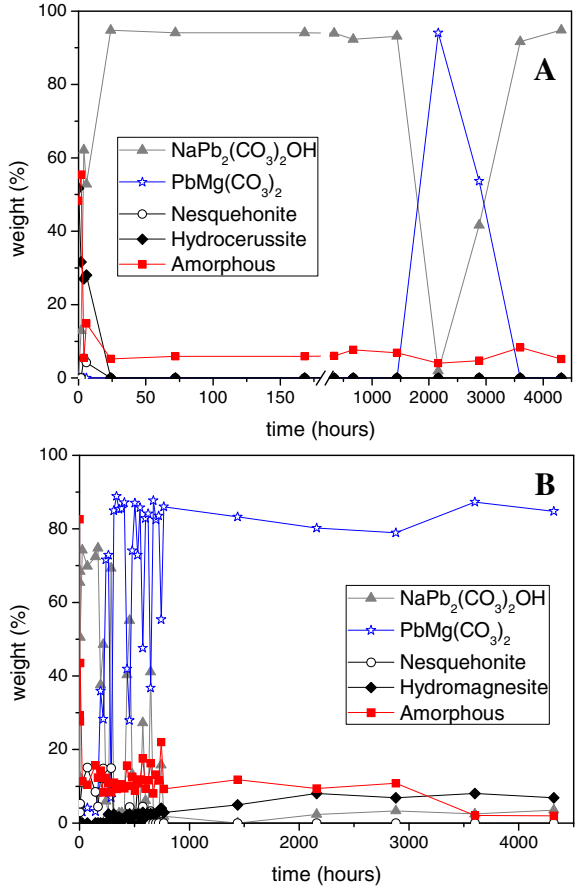

Fig. 6. Time evolution of weight% of the solid phases for: (A) Exp. Pb1; and (B) Exp. Pb2. Since nitratine appears as a result of the drying of the precipitates, it has been removed from the plots. Cerussite has also been removed from B due to its low amount (less than 1%).

4. DISCUSSION

The results shown in the previous section indicate that dolomite-analogues, norsethite and $PbMg(CO_3)_2$ form at room temperature by sequences of dissolution–crystallisa tion reactions which mainly depend on the Ba:Mg and Pb:Mg ratios in the slurries formed by mixing the parent solutions. Following the initial precipitation of a gel, disso lution–crystallisation reactions result in significant oscilla-tions in the relative amounts of precursor phases before norsethite or $PbMg(CO_3)_2$ become the main phases. Depending on the composition and stoichiometry of the slurries, the dissolution–precipitation process involved an amorphous phase with variable composition and different crystalline precursors (witherite and eitelite to the forma-tion of norsethite, and nesquehonite, hydrocerussite/cerus-site and $NaPb_2(CO_3)_2OH$ to the formation of $PbMg(CO_3)_2$).

In the case of norsethite formation, the precursor phases are different from those identified in previously reported experiments (see Pimentel and Pina, 2014a). Whereas eitelite is a minor phase but it seems to play a role in the formation of norsethite, hydromagnesite seems to crystallise from eitelite. This is supported by results of previous studies that have shown that reversible transfor-mations between eitelite and hydromagnesite may occur when the carbonate concentrations vary in the crystallisa-tion medium (Paine, 1997; Montes-Hernandez et al., 2012). Finally, nesquehonite was only detected in the precipitates removed after 4 h of ageing, indicating that it is not a precursor phase of norsethite either. Presumably, nesquehonite precipitates due to the large excess of Mg^{2+} and CO_3^{2-} in the slurries. Nevertheless, the high number of phases identified and their dependence on the starting conditions (Ba:Mg ratio) revealed that norsethite can be formed by a reaction involving an amorphous phase and witherite or, alternatively, by a reaction between a different amorphous phase and eitelite.

Unlike the experiments presented in Section 3.1, Pimentel and Pina (2014a) used solutions containing $BaCl_2$ and $MgCl_2$, instead of $Ba(NO_3)_2$ and $Mg(NO_3)_2$. A s a result, a different assemblage of precursor phases was iden-tified, i.e. witherite and northupite ($Na_3Mg(CO_3)_2Cl$). Interestingly, previous experiments using the same Ba:Mg ratio as in Exp. Ba1 resulted in similar oscillations in the relative amount of precursor phases of highly crystalline norsethite (Pimentel and Pina, 2014a). Together, these experimental results demonstrate that different pathways towards the formation of norsethite by the coupling of dis solution–crystallisation reactions are possible.

In the two experiments designed to crystallise $PbMg(CO_3)_2$, a similar initial mineral assemblage composed of nesquehonite, hydrocerussite/cerussite and $NaPb_2(CO_3)_2OH$ was identified, but two different crystallisation path-ways were observed. In Exp. Pb1 (i.e. the experiment with the higher Pb:Mg ratio), $PbMg(CO_3)_2$ forms from $NaPb_2(CO_3)_2OH$ and an amorphous phase. Subsequently, $PbMg(CO_3)_2$ dissolves until its complete disappearance. Assum-ing that $PbMg(CO_3)_2$ is the stable phase, this suggests that in Exp. Pb1 chemical equilibrium was not reached after 6 months of slurry ageing. In contrast, for Exp. Pb2, once $PbMg(CO_3)_2$ is formed from the precursor phases after ~7 days, it remains stable and the minor phase nesque-honite disappears in less than a month of ageing, suggesting a subsequent nesquehonite–hydromagnesite transformation (Davies and Bubela, 1973). These two different reaction pathways towards $PbMg(CO_3)_2$ indicate that there are at least two different sequences of dissolution–crystallisation reactions toward the formation of this dolomite-analogue.

The slower kinetics of $PbMg(CO_3)_2$ formation com-pared to that of norsethite, may indicate structural con-straints related to differences in the size of the constituting cations of dolomite-analogues. According to Lippmann (1973), Ca^{2+} and Mg^{2+} in the dolomite structure are both octahedrically coordinated to oxygen atoms of the carbonate groups. In a different way, Mg^{2+}, and Ba^{2+} and Pb^{2+} show different coordination polyhedra in the nor-sethite and $PbMg(CO_3)_2$ structures. Whereas in these struc-tures, Mg^{2+} remains octahedrically coordinated to oxygen atoms, Ba^{2+} and Pb^{2+} are surrounded by twelve oxygen atoms and the coordination polyhedra can be described by a distorted ditrigonal prism (Lippmann, 1973). This means that, unlike dolomite, norsethite and $PbMg(CO_3)_2$

structures are formed by an alternation of cations with different coordination schemes, which can favour cationic ordering along the c-axis. Since the radius of Ba^{2+} (1.38 Å) is larger than the radius of Pb^{2+} (1.26 Å), the cor-responding coordination polyhedra in the crystal structure of norsethite are larger than in the structure of $PbMg(CO_3)_2$. The smaller relative size of the Pb^{2+} and Mg^{2+} coordination polyhedra in the closer $PbMg(CO_3)_2$ structure seems to hinder its formation. Certainly, this qualitative explanation of the different kinetics of norsethite and $PbMg(CO_3)_2$ formation is still speculative, but it is sup-ported by the fact that to date it was not possible to synthe-sise the dolomite-analogue $SrMg(CO_3)_2$, which has an even smaller relative size of coordination polyhedra than $PbMg(CO_3)_2$, by mixing solutions at room temperature (negative experimental results not shown here).

The strong difference in the crystallisation kinetics exhibited by the dolomite-analogues poses another funda-mental question on the role played by the hydration of Mg^{2+} in the formation of dolomite and dolomite-analogues. Since the formation of all dolomite-like struc-tures requires an equal incorporation of magnesium, the inhibition of dolomite crystallisation at room temperature cannot be exclusively attributed to the high dehydration barrier of Mg^{2+} ions. This conclusion has been recently supported by experiments designed to crystallise dolomite from non-aqueous solutions (Xu et al., 2013). Furthermore, the similar diffusion coefficients of Ba^{2+} ($8.48\cdot10^{-6}$ cm^2/s), Pb^{2+} ($9.45\cdot10^{-6}$ cm^2/s), Mg^{2+} ($7.05\cdot10^{-6}$ cm^2/s), and Ca^{2+} ($7.93\cdot10^{-6}$ cm^2/s) in water at 25 □C (Li and Gregory, 1974), makes it difficult to explain exclusively in terms of ionic mobility the very different crystallisation kinetics of dolomite and dolomite-analogues. Therefore, we propose that the shape and relative size of coordination polyhedra of constituting cations (i.e. Mg^{2+}, Ca^{2+}, Ba^{2+}, Pb^{2+} and Sr^{2+}) play a fundamental role in the formation of double carbonates with dolomite-like structures at ambient conditions.

5. CONCLUSIONS

Norsethite and $PbMg(CO_3)_2$ were crystallised at ambi-ent conditions by ageing slurries formed from mixing solu-tions of $Ba(NO_3)_2$, $Pb(NO_3)_2$, $Mg(NO_3)_2$ and Na_2CO_3. To the best of our knowledge, this is the first report of the syn-thesis of $PbMg(CO_3)_2$ using the solution-mixing method. Depending on the initial cationic ratios in the slurries (i.e. Ba:Mg and Pb:Mg), a number of pathways towards the formation of these dolomite-analogues have been iden-tified and monitored. These pathways show a stage, in which the relative amounts of the precursor phases oscil-late. The evolution of the composition of the slurries seems to indicate that the formation of the studied dolomite-analogues occurs by the sequential coupling of dissolu tion–crystallisation reactions. Whereas oscillations in nor-sethite experiments typically last 24 h, oscillations associ-ated to the $PbMg(CO_3)_2$ formation occur for periods of time longer than one month.

The different kinetics of formation of norsethite and PbMg(CO3)2 indicate that structural constraints due to the relative size of the constituting cations of these double carbonates could be a more relevant factor than the magnesium hydration in determining the time scale for crystallisation of dolomite-like structures. Therefore, future experimental and theoret-ical investigations on the effect of structural constraints on the crystallisation kinetics of dolomite-analogues could provide new insights into the long-standing problem of dolomite formation in nature.

ACKNOWLEDGMENTS

This work was supported by the Spanish Government (MAT2012-38810 and CGL2013-48247-P). SEM images and EDX analyses were obtained at the ICTS Centro Nacional de Microscopia Electro´nica, (UCM). Authors wish to thank Bele´n Soutullo and Jorge Moreno for technical support. Carlos Pimentel is grateful to the Spanish Government for a FPU Fellowship. This paper benefited from insightful comments by Alfonso Mucci and three anonymous reviewers.

APPENDIX A. SUPPLEMENTARY DATA

Supplementary data associated with this article can be found, in the online version, at http://dx.doi.org/10.1016/ J· gca.2015.12.040.

REFERENCES

Bo¨ttcher M. E. (2000) Stable isotope fractionation during experimental formation of norsethite ($BaMg[CO_3]_2$): a mineral analogue of dolomite. Aquatic Geochemistry 6, 201–212. http://dx.doi.org/10.1023/A:1009646805933.

Bo¨ttcher M. E., Gehlken P. L., Skogby H. and Reutel C. (1997) The vibrational spectra of $BaMg(CO_3)_2$ (norsethite). Mineralogical Magazine 61, 249–256.

Crespo A., Pimentel C. and Pina C. M. (2015) Ana´lisis Cristaloqui´mico y Tratamiento Te´rmico de Algunas Dolomitas Naturales. Macla 20, 37–38 (In Spanish).

Chung F. H. (1974) Quantitative interpretation of X-ray diffraction patterns of mixtures. I. Matrix-flushing method for quantitative multicomponent analysis. Journal of Applied Crystallography 7, 519–525.

Davies P. J. and Bubela B. (1973) The transformation of nesquehonite into hydromagnesite. Chemical Geology 12, 289–300. Deelman J. C. (2011) Low-temperature Formation of Dolomite and Magnesite, Version 2.3, 512 p..

Hood W. C., Steidl P. F. and Tschopp D. G. (1974) Precipitation of norsethite at room temperature. American Mineralogist 59, 471–474.

Hubbard C. R. and Snyder R. L. (1988) RIR-measurement and use in quantitative XRD. Powder Diffraction 3, 74–77.

Kelleher I. J. and Redfern S. A. T. (2002) Hydrous calcium magnesium carbonate, a possible precursor to the formation of sedimentary dolomite. Molecular Simulations 28, 557–572.

Li Y.-H. and Gregory S. (1974) Diffusion of ions in see water and in deep-sea sediments. Geochimica et Cosmochmica Acta 88, 708–714.

Lippmann F. (1966) $PbMg(CO_3)_2$, ein neues rhomboedrisches Doppelcarbonat. Die Naturwissenschaften 24, 701.

Lippmann F. (1967) Die Synthese des Norsethits, $BaMg(CO_3)_2$, bei ca. 20 und 1at. ein Modell zur Dolomitisierung. Neues Jahrb. Mineral. Monatsh 12, 23–29.

Lippmann F. (1973) Sedimentary Carbonate Minerals. Springer-Verlag, 228 p..

Martin J. D. (2008) A Software Package for Powder X-ray Di*ff*raction Analysis, ISBN: 84-609-1497-6.

McKenzie J. A. (1981) Holocene dolomitization of calcium carbonate sediments from the coastal sabkhas of Abu Dhabi, U.A.E.: a stable isotope study. Journal of Geology 89, 185–198. Montes-

Hernandez G., Renard F., Chiriac R., Findling N. and Toche F. (2012) Rapid precipitation of magnesite microcrystals from $Mg(OH)_2$–H_2O–CO_2 slurry enhanced by NaOH and a heat-aging step (from ∼20 to 90 □C). Crystal Growth and Design 12, 5233–5244. http://dx.doi.org/10.1021/cg300652s.

Morrow D. W. and Ricketts B. D. (1986) Chemical controls on the precipitation of mineral analogues of dolomite: the sulfate enigma. Geology 14, 408–410.

Paine J. B. (1997) Use of Eitelite to Reduce Sidestream Smoke. Available at: http://www.google.es/patents/US5699811.

Parkhurst D. L. and Appelo C. A. J. (2013) Description of Input and Examples for PHREEQC Version 3 – A Computer Program for Speciation, Batch-reaction, One-dimensional Transport, and Inverse Geochemical Calculations. U.S. Geological Survey Techniques and Methods (book 6, chapter A43, 497 pp.).

Pimentel C. and Pina C. M. (2014a) The formation of the dolomite-analogue norsethite: reaction pathway and cation ordering. Geochimica et Cosmochmica Acta 142, 217–233. http://dx.doi.org/10.1016/j.gca.2014.07.021.

Pimentel C. and Pina C. M. (2014b) Formacio´n de Minerales Ana´logos a la Dolomita. Macla, 19 pp. (in Spanish).

Rodriguez-Blanco J. D., Shaw S. and Benning L. G. (2015) A route for direct crystallization of dolomite. American Mineralogist 100, 1172–1181.

Schultz-Gu¨ttler R. (1986) The influence of disordered, non-equilibrium dolomites on the Mg-solubility in calcite in the system $CaCO_3$–$MgCO_3$. Contributions to Mineralogy and Petrology 93, 395–398.

Song R. Q., Xu A. W., Antonietti M. and Co¨lfen H. (2009) Calcite crystals with platonic shapes and minimal surfaces. Angewandte Chemie 48, 395–399.

Xu J., Yan Ch., Zhang F., Konishi H., Xu H. and Teng H. (2013) Testing the cation-hydration effect on the crystallization of Ca–Mg–CO_3 systems. Proceedings of the National Academy of Sciences 110, 17750–17755.